



## Impact of Ho and Ce Ions Substitution on Structural, Electrical, and Dielectric Properties of Ni-Zn Ferrites

Alina Manzoor<sup>1\*</sup>, Aqib Javed<sup>1</sup>, Amir Muhammad Afzal<sup>2</sup>, M. Imran Arshad<sup>1</sup>, Aamir Shahzad<sup>1</sup>

<sup>1</sup> Department of Physics, Government College University, Faisalabad, 38000, Pakistan

<sup>2</sup> Department of Physics, Riphah International University, 13-Km Raiwind Road, Lahore-54000 Pakistan

### ARTICLE INFO

### ABSTRACT

#### Article History:

Received: May 14, 2020

Revised: June 16, 2020

Accepted: June 29, 2020

Available Online: June 30, 2020

#### Keywords:

XRD

Nanoparticles

Dc resistivity

FTIR spectroscopy

Dielectric properties

In the present study, influence of holmium (Ho) and cerium (Ce) ions on the electromagnetic properties of  $\text{Ni}_{0.67}\text{Zn}_{0.33}\text{Fe}_{1.9}\text{Ho}_{0.1-x}\text{Ce}_x\text{O}_4$  ferrites ( $x = 0, 0.025, 0.05, 0.075, 0.1$ ) synthesized by the self-ignited sol-gel method was studied. The XRD experiment was performed to determine the substitutional effects on structural parameters. FTIR spectroscopy and I-V measurements were carried out to analyze the spectral and electrical behavior of substituted samples. X-ray diffraction patterns revealed the FCC structure of the prepared samples. The value of average crystallite size was noticed between 25.89-39.51 nm, while lattice constant was found in the range 8.37-8.41 Å. Both the low and the high frequency absorption bands were confirmed by FTIR technique. Tetrahedral band was noted in the range 463-495  $\text{cm}^{-1}$  while octahedral band was observed in range 558-560  $\text{cm}^{-1}$ . The dc resistivity was observed to decrease with increase in temperature which indicates the semi-conductor like behavior of the prepared samples. Dielectric study showed that both the dielectric constant and the tangent loss factor were decreased with rise in the applied field frequency.

### OPEN ACCESS

© 2020 The Authors, Published by iRASD. This is an Open Access article under the Creative Common Attribution Non-Commercial 4.0

\*Corresponding Author's Email: [alinamanzoor@gmail.com](mailto:alinamanzoor@gmail.com)

## 1. Introduction

The launch of nano-crystalline magnetic materials has opened up a new era in the history of magnetism. Magnetic materials at the nanoscale are the foundation of the innovation of recent time. It is some of the time taken that the progressive accomplishments of today technology are truly not cell phones, satellite and space communication, or super-fast trains; it is essentially the capability to introduce those materials which are actually the fundamental parts for various technological and modern applications. The nano structured magnetic oxide materials now a days have become the center of interest due to their novel applications and noteworthy tremendous properties (Hashim et al., 2012). Nano-sized soft ferrites, among all the present magnetic materials have drawn the attention of today researchers for not only their flexible and testing uses in density recording media, microwave frequency based devices, and data processing strategies, yet likewise their rare and matchless properties, for example, redistribution of cations and super paramagnetism (SPM) in contrast to their bulk matches (Randhawa & Singh, 2013).

The cubic ferrites are found to be incredibly unique materials due to the extraordinary features such as superparamagnetic nature, extraordinary permeability, low magnetic losses, great thermo-chemical stability, low eddy losses, high dc resistivity, large saturation magnetization, and single area conduct which can be upgraded by tuning the material processing methods as well as the response conditions. All the above-mentioned

unique properties manage the cost of these materials in ultrahigh frequency applications that require strong connection to the electromagnetic signals while offering the minimal losses (Dar, Shah, Siddiqui, & Kotnala, 2012; Ferrites, 2012). The surface properties perform a leading role as compared to core in managing the physical and chemical features of nano materials (Alone, Shirsath, Kadam, & Jadhav, 2011). For high-performance devices, a basic need is to manufacture the ferrite materials at nano scale. Below a critical size, soft ferrites act like single-domain systems. The domain wall resonance effect is maintained at critical size, and material can offer high efficiency at higher frequencies (Rao et al., 2006). Soft ferrites also known as cubic ferrites possess a general formula  $\text{MeFe}_2\text{O}_4$ , where 'Me' can be a trivalent or a divalent ion. The cubic phase Ni-Zn cubic ferrite is among one of the notable and most substantial kinds of soft ferrites which possess large saturation magnetization ( $M_s$ ), high Curie temperature, and high dc Resistivity (Akhter & Hakim, 2010). One way to improve their electrical conductivity, structural, dielectric, and electromagnetic properties is to substitute rare earth cations ( $\text{Ho}^{3+}$ ,  $\text{La}^{3+}$ ,  $\text{Er}^{3+}$ ,  $\text{Ce}^{3+}$ , etc) on octahedral sites (Cai, Wang, et al., 2016; Cai, Xu, et al., 2016; Iqbal, Islam, Ali, Sadiq, & Ali, 2014). Secondly, a great deal of improvement has been believed to understand different synthetic and physical phenomenon associated with substituted Ni-Zn ferrites. The profoundly resistive Ni-Zn nano-ferrites alongside reasonable incorporation of trivalent, divalent, and rare earth (RE) cations have discovered unique thought by various experts because of huge practical assorted variety of appropriately substituted Ni-Zn ferrites. As discussed earlier by A. Ghafoor et al that dc electrical resistivity increased by doping of holmium ions, yet the saturation magnetization also reduced by 32 % and increase in coercivity was predicted.

Holmium (Ho) and cerium (Ce) being rare earth elements possess high electrical resistivity as well as large magnetic permeability (Manzoor, Khan, Shahid, & Warsi, 2017). Here, in the present study, we expect to examine the substitutional effects of Ce and Ho ions into the Ni-Zn structure which has never been concentrated before. Subsequently, to address the issue of low loss and highly resistive materials, we propose the Ho and Ce doped Ni-Zn ferrites via size-monitored sol-gel method. The current work is the study of Ho and Ce doped Ni-Zn ferrites to reveal the substitutional consequences for microstructure, cations redistribution, optical, electrical, and dielectric characteristics. Remarkably, when Ce and Ho ions are introduced in nickel-based magnetic oxides, the substitute of Fe by larger sized Ce and Ho ions differ the basic structural, spectral, electrical, and dielectric parameters.

## 2. Experimental

$\text{Ni}_{0.67}\text{Zn}_{0.33}\text{Fe}_{1.9}\text{Ho}_{0.1-x}\text{Ce}_x\text{O}_4$  ( $x = 0.00-0.1$ ) nano-sized ferrites doped with Ho and Ce were prepared through a self-ignited sol-gel method. The stoichiometric volumes of  $\text{Ni}(\text{NO}_3)_2 \cdot 6\text{H}_2\text{O}$ ,  $\text{Fe}(\text{NO}_3)_3 \cdot 9\text{H}_2\text{O}$ ,  $\text{Zn}(\text{NO}_3)_2 \cdot 6\text{H}_2\text{O}$ ,  $\text{Ho}(\text{NO}_3)_3 \cdot 5\text{H}_2\text{O}$  and  $\text{Ce}(\text{NO}_3)_3$  were taken in distilled water. After a homogeneous mixing of all salts, citric acid was added at 40 °C with salts to citric acid ratio of 1:2 subject to constant mixing. The addition of citric acid being a natural chelating agent can help to chelate the metal particles with alterable ionic dimensions and forestalling precipitation to protect the uniformity among the ingredients. Next to that, precipitate formation was avoided by raising the pH of the solution by adding 2M ammonia solution. The solution was then heated at 90 °C under constant stirring after which a thick gel was acquired. By raising temperature as far as 150 °C, the auto-ignition of thick gel took place, and a furry dark gray material was obtained. After the well grinding of obtained material, the sintering was conducted at 900 °C for 6 hr for the elimination of natural residues and for the formation of cubic phase. Circular shaped pellets of 13.55 mm diameter were made below 30 KN pressure using hydraulic Press. The XRD patterns of annealed samples were taken to examine the structural parameters and fcc phase confirmation by X-ray diffractometer (D8 Advance-Bruker) at room temperature. FTIR spectra were taken from 400 -to 1000  $\text{cm}^{-1}$  utilizing Nicolet spectrometer (TM 5700) at room-temperature. Room-temperature dielectric study was carried out on pellets samples utilizing Wayne Ker impedance analyzer (WK6500B) from 1 MHz -to 3 GHz. The dc resistivity was determined by two probe technique.

### 3. Results and Discussion

#### 3.1. X-Ray Diffraction Analysis

The recorded XRD scans of  $\text{Ni}_{0.67}\text{Zn}_{0.33}\text{Fe}_{1.9}\text{Ho}_{0.1-x}\text{Ce}_x\text{O}_4$  ( $0.0 \leq x \leq 0.1$ ) nano particles calcinated at 900 °C are presented in figure 1. The presented XRD patterns revealed the Bragg diffractions of fcc structure relating to Fd3m space group (AsifIqbal et al., 2017). The XRD graph of the sample with  $x=0$  shows the formation of fcc single phase with all necessary reflection peaks having hkl (220), (311), (400), and (511) as verified by ICDD No: 00-010-0325. No extra peaks other than the fcc phase  $x=0.00$  assured the formation of single-phase fcc structure. Though, the substitution of Ho and Ce inside Ni-Zn lattice influences the spinel network and prompts the presence of an impurity phase ( $\text{HoFeO}_3$ ) defined by ICDD No: 00-010-0325. The broadening of reflection peaks is noted for samples with  $x \geq 0.025$ . No traces of secondary phase are identified for  $x=0.1$  and for the sample in which both holmium and cerium doping is absent. The diffraction peak (311) is found to be broaden by increasing the value of  $x$ . Various structural quantities like lattice constant ( $a$ ), porosity ( $P$ ), cell volume ( $a^3$ ), and densities (hypothetical and mass) are affected by  $\text{Ho}^{3+}$  and  $\text{Ce}^{3+}$  contents.

The lattice constant 'a' is calculated using Nelson-Riley function (Ali et al., 2012) and its variation is plotted with respect Ho and Ce content in  $\text{Ni}_{0.67}\text{Zn}_{0.33}\text{Fe}_{1.9}\text{Ho}_{0.1-x}\text{Ce}_x\text{O}_4$  ferrites. The lattice constant is examined to increase with the addition of Ho and Ce ions which is attributed to the larger ionic radii of Ho and Ce ions on octahedral sites. The average crystalline size is determined from the widening of the diffraction peaks by Debye Scherrer's formula.

$$D = k\lambda/\beta\cos\theta \quad (1)$$

Here, D represents the value of average crystalline size, which is measured in nm,  $\beta$  is FWHM measured in radians, k is some constant ( $= 0.94$ ),  $\theta$  is the Bragg's angle and  $\lambda$  is the known wavelength. The average crystallite size value is observed from 39.51 -to 25.89 nm. The theoretical ( $\rho_b$ ) and experimental density ( $\rho_x$ ) are determined by the following equations.

$$\rho_b = m/\pi r^2 h \quad (2)$$

$$\rho_x = 8M/Na^3 \quad (3)$$

Here M is the atomic weight, N is the Avogadro's number, a shows the lattice constant, m is the pellet's mass, h is the thickness and r is the radius of the pellet. As it is clear from above equation that X-ray density relies upon the molecular weight and the lattice constant of the material, its value increases from 4.74 -to 6.33  $\text{g/cm}^3$  with increasing the Ho and Ce concentrations. This pattern is normal as molecular weight of holmium (164) and Ce (140) are higher than that of the iron (56). Similarly, the bulk density  $\rho_b$  is raised from 2.64 -to 3.94  $\text{g/cm}^3$  with Ho and Ce substitution. Since the density value of the iron (7.87 $\text{g/cm}^3$ ) is less than the holmium (8.8  $\text{g/cm}^3$ ) than so a denser structure is expected to form by increasing the Ho ions. The values of X-ray density are bigger than the bulk density which might be credited to the pores formed during the calcination procedure what's more of improved densification and grains development upon Ho and cerium consolidation substitution (Haque, Huq, & Hakim, 2008). The percentage porosity (P %) is calculated using  $\rho_x$  and  $\rho_b$  via following relation;  $P \% = 100 (1 - \rho_b/\rho_x)$ . The percent porosity is noted to reduce from 44.6 to 23.2 %, as the X-ray density has greater magnitudes than bulk density as well as the increase with Ho and Ce ions incorporation. The formation of ortho-phase ( $\text{HoFeO}_3$ ) covered the inter-granular cavities which results in high compression, so a decline in P is assuming upon Ce and Ho substitution. Figure 2 illustrates the change in lattice constant with respect to Ho and Ce concentration.

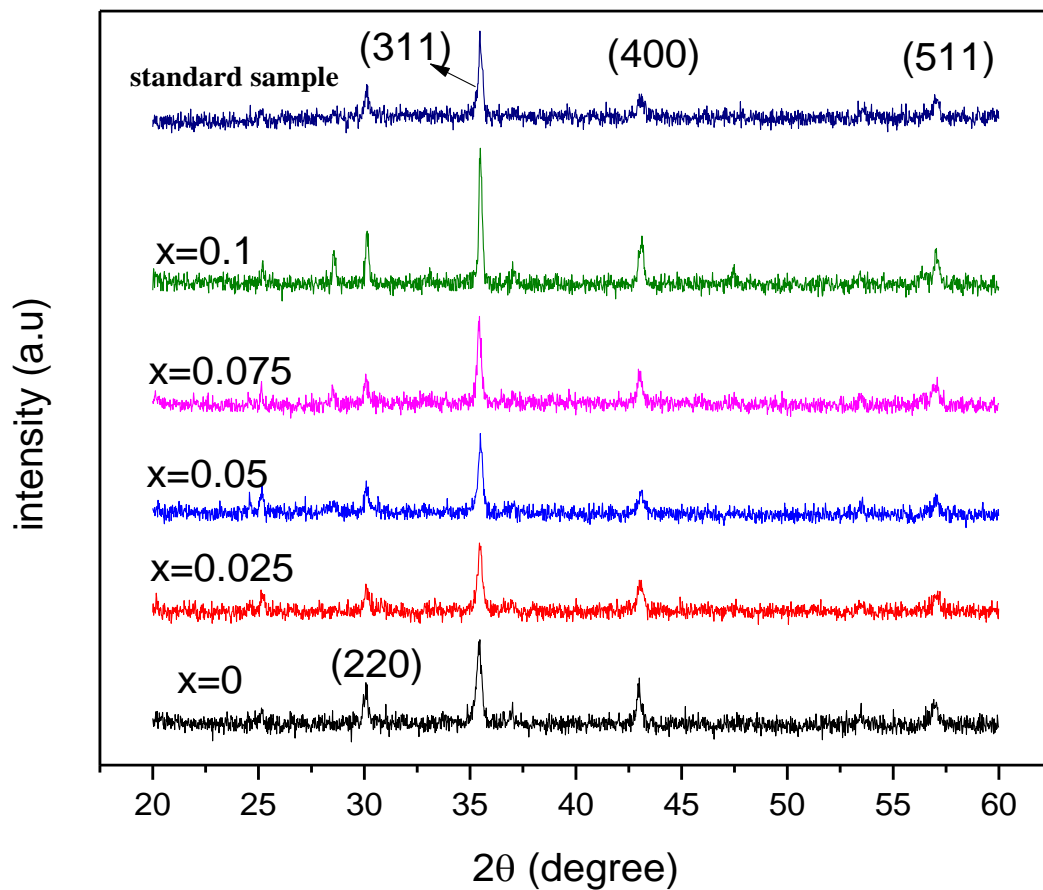


Figure 1: Combined XRD graphs of Ni-Zn soft ferrites

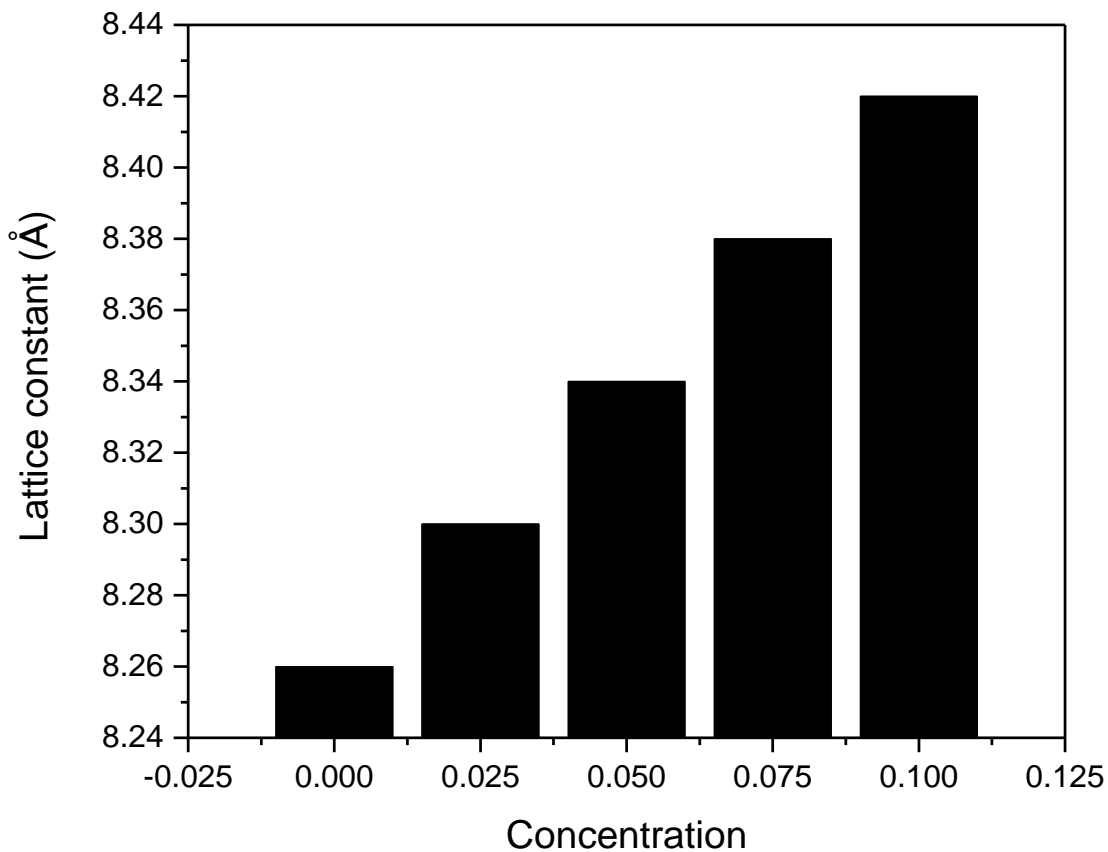


Figure 2: Graph between Ho, Ce concentration and lattice constant

### 3.2. FTIR Studies

The qualitative information regarding materials' structure and local symmetry of crystalline solids is provided by Infrared absorption spectroscopy. Figure 3 represents the FTIR scans for all  $\text{Ni}_{0.67}\text{Zn}_{0.33}\text{Fe}_{1.9}\text{Ho}_{0.1-x}\text{Ce}_x\text{O}_4$  samples. The scan range is taken from 400 -to 1000  $\text{cm}^{-1}$ . The growth of the spinel phase is validated by the taken FTIR spectra. Two distinct intrinsic frequency peaks are observed in the defined range arising due to the vibrations of oxygen-bonds and metal-cations. The intrinsic band  $u_1$  at relatively higher wave number (550 - 600  $\text{cm}^{-1}$ ) represents the oxygen ions bond and octahedral metal-cation vibrations, while intrinsic band  $u_2$  at lower frequency (450 - 500  $\text{cm}^{-1}$ ) show up the oxygen bond and tetrahedral metal-cation stretching vibrations (Ramesh, Rao, Samatha, & Rao, 2015). For  $x=0$ , the octahedral ( $u_1$ ) and tetrahedral ( $u_2$ ) vibrational groups are revealed at 600  $\text{cm}^{-1}$  and 450  $\text{cm}^{-1}$ . The following relations can determine the force constants of octahedral and tetrahedral sites ( $K_o$  &  $K_t$ ).

$$K_o = 0.94213 M (u_2)^2 / (M + 32) \quad (4)$$

$$K_t = 2^{(1/2)} K_o (u_1/u_2) \quad (5)$$

Here 'M' is the atomic weight of the particular composition.

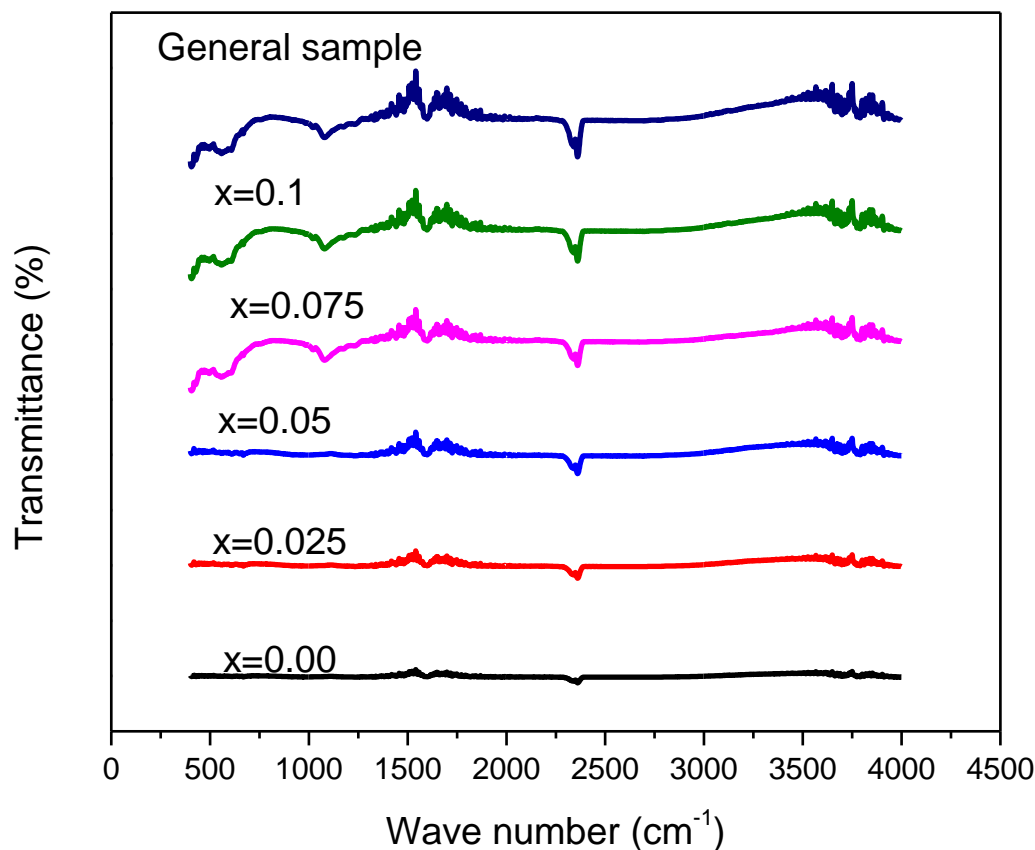


**Figure 3: FTIR Spectra of  $\text{Ni}_{0.67}\text{Zn}_{0.33}\text{Fe}_{1.9}\text{Ho}_{0.1-x}\text{Ce}_x\text{O}_4$  ( $x = 0.00-0.1$ ) ferrites**

A reduction in  $K_o$  and  $K_t$  is observed up to  $x = 0.06$  and after that their values increased with rising the  $\text{Ho}^{3+}$  and  $\text{Ce}^{3+}$  concentration. It is also seen that the behavior of force constant is in consistent with bond lengths ( $r_A$  and  $r_B$ ) which is ascribed to the reality that less energy is needed to break down the longer bindings and the other way around (Srivastava & Srinivasan, 1982).

### 3.3. Dielectric Studies

The dielectric properties of  $\text{Ni}_{0.67}\text{Zn}_{0.33}\text{Fe}_{1.9}\text{Ho}_{0.1-x}\text{Ce}_x\text{O}_4$  ( $x=0.00-0.1$ ) ferrites have been examined from 1MHz -to 3GHz. Figure 4 shows the variation of dielectric constant ( $\epsilon'$ ) as a function of frequency at room-temperature. The dielectric constant exhibits high values

at shorter frequency and then reduces quickly by increasing the frequency. Such type of conduction has additionally been seen in different reaction of ferrite frameworks when exposed to the applied electric field. This type of conduction is characterized as Debye type conduction which occurs when the charge transporters go through the space-charge polarization impact as supported by the Koop's theory. Ferrite materials are viewed as conducting-grains partitioned by relatively thin grain-boundaries (more resistive than grains) (Koops, 1951). In ferrites, the source of polarization predominantly originates from four essential procedures: interfacial, dipolar, electronic, and ionic polarizations. The reason of conduction in spinel ferrites is basically the electron jumping between  $\text{Fe}^{2+}$  and  $\text{Fe}^{3+}$  ionic states at octahedral sites. For low field region the electrons heap up at inner interfaces because of poor leading resistive grain boundaries and hence creating space-charge polarization (Livingston, 1999). By enhancing the applied field, the path of electron movements turned around before accumulating at boundaries which diminishes the possibility of electrons to move at grain boundaries. Henceforth, conduction phenomenon and dielectric permittivity observed to decrease (Singh, Agarwal, & Sanghi, 2011). The undamped dipoles caused some resonance peaks at  $f \sim 2$  GHz (Harrop & Campbell, 1968). The maximum in dielectric constant happens under the following situation.

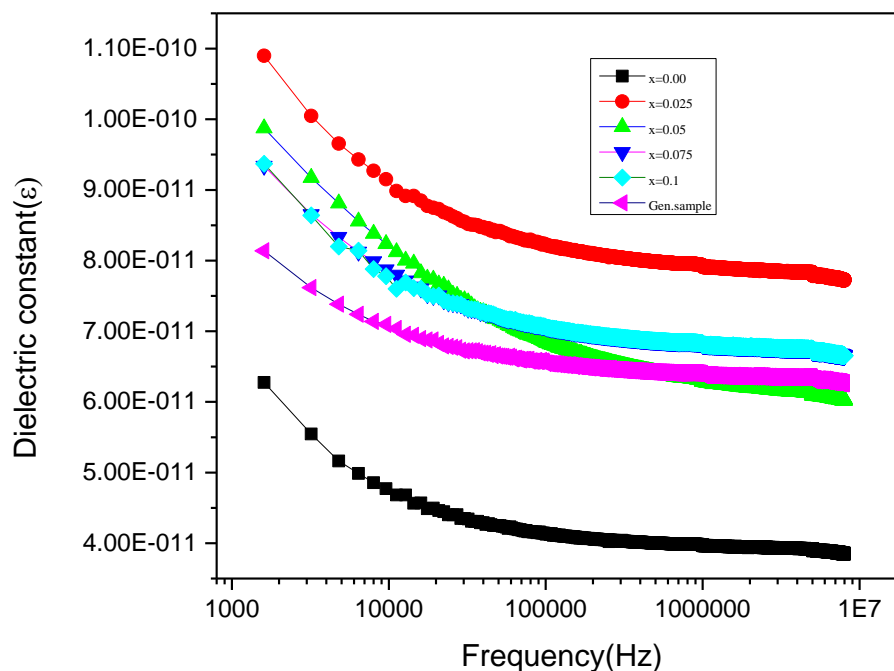


**Figure 4: Frequency vs dielectric constant of  $\text{Ni}_{0.67}\text{Zn}_{0.33}\text{Fe}_{1.9}\text{Ho}_{0.1-x}\text{Ce}_x\text{O}_4$  ( $x = 0.00-0.1$ ) ferrites**

$$\omega_{\max} \tau = 1$$

(6)

Where  $\tau$  is the relaxation time and  $\omega_{\max}$  is the angular frequency equal to  $2\pi f_{\max}$ . When the electron's bouncing rate approaches to the applied field rate then Debye relaxation occurs, also called the ferrimagnetic resonance (Ashiq, Iqbal, & Gul, 2011). The applied field frequency at which polarity shifting of ions takes place is named as natural frequency. When both the natural and applied field frequencies remunerate one another, maximum electrical energy is moved to oscillating ions following a rise in power dissipation. Consequently, a resonance happens as can be seen by the resonance heights (Zhou, Li, & Chen, 2010). The addition of  $\text{Ho}^{3+}$  and  $\text{Ce}^{3+}$  ions at octahedral sites decreases the  $\text{Fe}^{3+}$  ions residing there, delivering an adjustment in polarization. By increasing cerium and holmium contents at octahedral sites, a drop in hopping movement of electrons take place which diminishes the agglomeration of electrons at the grain boundaries and, subsequently, hindering the growth of space-charge polarization. It can be realized from figure 4 that the variation of  $\epsilon'$  with  $\text{Ho}^{3+}$  and  $\text{Ce}^{3+}$  substitution isn't consistent. The  $\epsilon''$  and  $\epsilon'$  have values from 0.17 -to 0.77 and 2.54 -to 4.0 respectively, while for  $x= 0.12$  the greatest values of  $\epsilon'$  and  $\epsilon''$  are noted. This kind of nonlinear change in dielectric constant with respect to substitutional ions has also been stated earlier (Cai, Xu, et al., 2016). There are various complicated parameters that influence the dielectric constant, such as electronic

polarization, ionic polarization, conductance losses, orientation as well as interface polarization (Fang, Ye, Zhang, & Xie, 2005).

The detected variation in dielectric constant may be supported in two aspects; after addition of  $\text{Ho}^{3+}$  and  $\text{Ce}^{3+}$  ions into spinel structure, the cations end up being progressively expanded and can form multi-dipoles with anions ( $\text{O}^{2-}$ ) to enhance the dipolar polarization (Abbas, Dixit, Chatterjee, & Goel, 2007). Moreover, the addition of  $\text{Ho}^{3+}$  and  $\text{Ce}^{3+}$  has successfully strengthened the  $\text{Fe}^{2+} \rightarrow \text{Fe}^{3+}$  shift to bring down the dielectric losses that results from the enhanced electron jumping. Furthermore, as the ionic radius of  $\text{Ho}^{3+}$  and  $\text{Ce}^{3+}$  are sufficiently greater than  $\text{Fe}^{3+}$  so the rise in lattice constant twists the lattice coming about an increment in the natural activity. Thus, conduction losses ( $\epsilon''$ ) have improved (Meena, Bhattacharya, & Chatterjee, 2010). The variations of tan loss and impedance as a function of frequency are shown in figures 5 & 6, respectively.

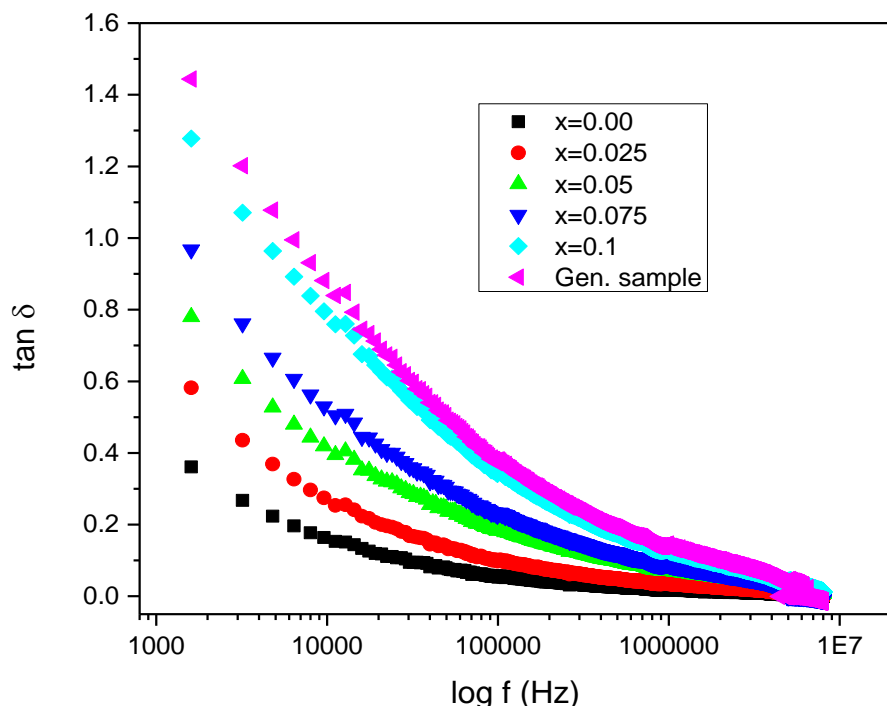


**Figure 5: Log f vs tangent loss of  $\text{Ni}_{0.67}\text{Zn}_{0.33}\text{Fe}_{1.9}\text{Ho}_{0.1-x}\text{Ce}_x\text{O}_4$  ( $x = 0.00-0.1$ ) ferrites**

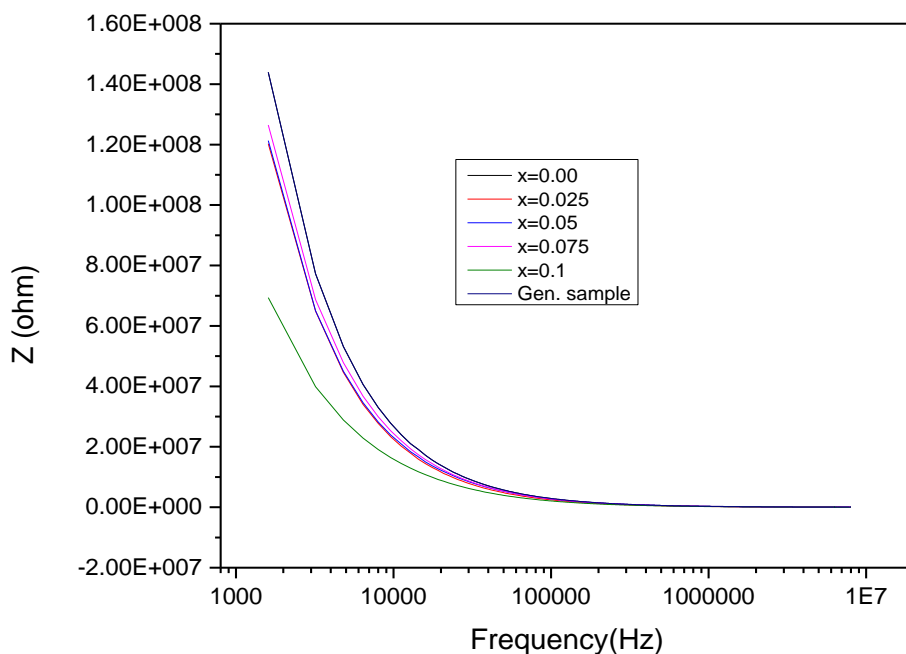


**Figure 6: Frequency vs impedance of  $\text{Ni}_{0.67}\text{Zn}_{0.33}\text{Fe}_{1.9}\text{Ho}_{0.1-x}\text{Ce}_x\text{O}_4$  ( $x = 0.00-0.1$ ) ferrites**

### 3.4. Electrical Properties

It is notable that the electrical characteristics of soft ferrites are exceptionally sensitive to stoichiometric ratios and imperfections (E. Rezlescu, Rezlescu, Popa, Rezlescu, & Pasnicu, 1997). The dc electrical resistivity variations of  $\text{Ni}_{0.67}\text{Zn}_{0.33}\text{Fe}_{1.9}\text{Ho}_{0.1-x}\text{Ce}_x\text{O}_4$  ( $x=0.00-0.1$ ) ferrites are appeared in Fig. 7. It can be seen that resistivity is increased by substituting Ho and Ce contents instead of iron. The holmium and cerium ions try to fill the octahedral sites because of their higher ionic radii. Consequently, the number of  $\text{Fe}^{3+}$  ions diminish at octahedral positions which causes a structural distortion. Because of  $\text{Ho}^{3+}$  and  $\text{Ce}^{3+}$  substitution at octahedral sites, the hopping rate of electrons exchange between  $\text{Fe}^{2+}$  and  $\text{Fe}^{3+}$  is decreased with the decline of  $\text{Fe}^{3+}$  ions which are accountable factors for conduction process in ferrites. Consequently, the electrical resistivity increases with the substitution of Ho and Ce ions.

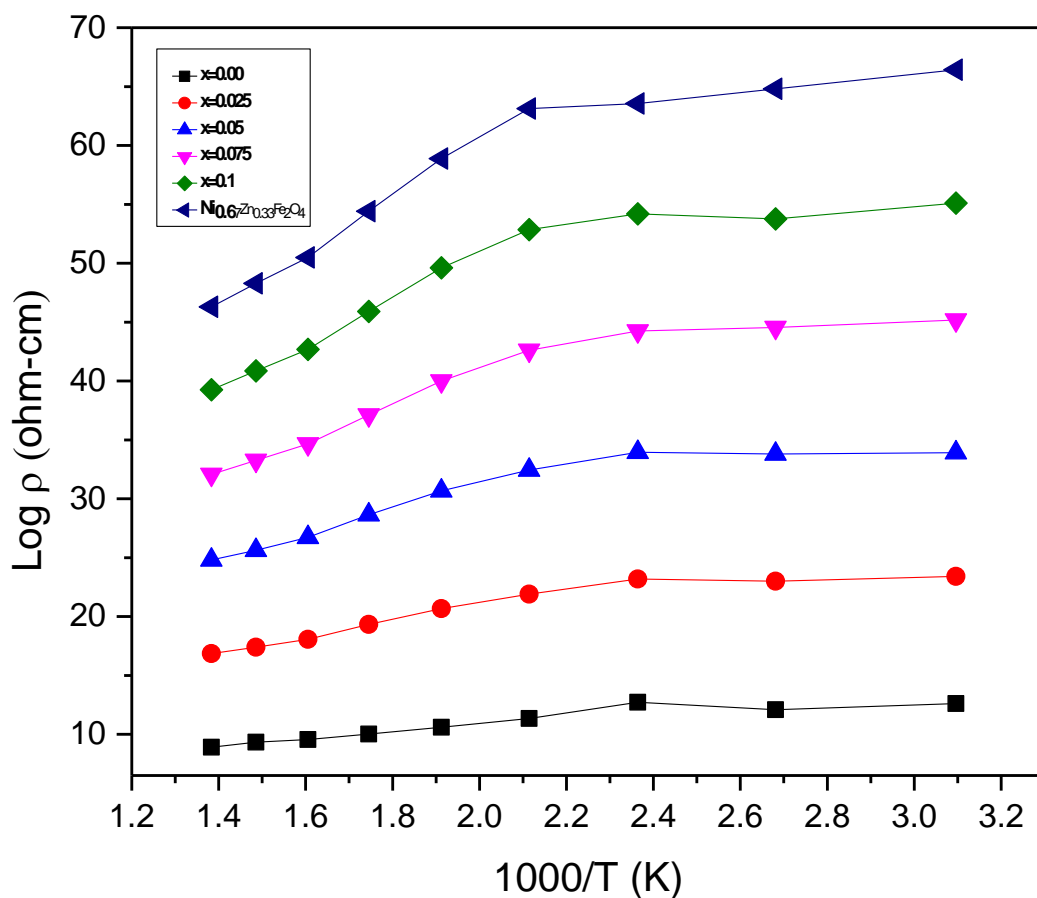


**Figure 7: 1000/T vs log of resistivity of  $\text{Ni}_{0.67}\text{Zn}_{0.33}\text{Fe}_{1.9}\text{Ho}_{0.1-x}\text{Ce}_x\text{O}_4$  ( $x = 0.00-0.1$ ) ferrites**

The rise in resistivity may be attributed to the higher resistivity values of Ho ( $221 \times 10^{-6} \Omega\text{-cm}$ ) when compared to that of Fe ( $9.98 \times 10^{-6} \Omega\text{-cm}$ ) (Koops, 1951). Temperature-dependent DC electrical resistivity plots of  $\text{Ni}_{0.67}\text{Zn}_{0.33}\text{Fe}_{1.9}\text{Ho}_{0.1-x}\text{Ce}_x\text{O}_4$  ferrites are displayed in figure 8. Each of the samples following the Arrhenius condition  $\rho = \rho_0 e^{\Delta E / K_B T}$  envisages the semiconductor nature of the materials, where  $\Delta E$  is the activation energy acquired from the straight fitting of Arrhenius plots (Sattar, El-Sayed, El-Shokrofy, & El-Tabey, 2005). The more extreme incline of log of resistivity versus  $1/T$  for each composition of  $\text{Ni}_{0.67}\text{Zn}_{0.33}\text{Fe}_{1.9}\text{Ho}_{0.1-x}\text{Ce}_x\text{O}_4$  can be seen because of the thermally initiated portability of charge carriers, yet not to a thermally activated creation of these carriers (N. Rezlescu, Rezlescu, Pasnicu, & Craus, 1994).

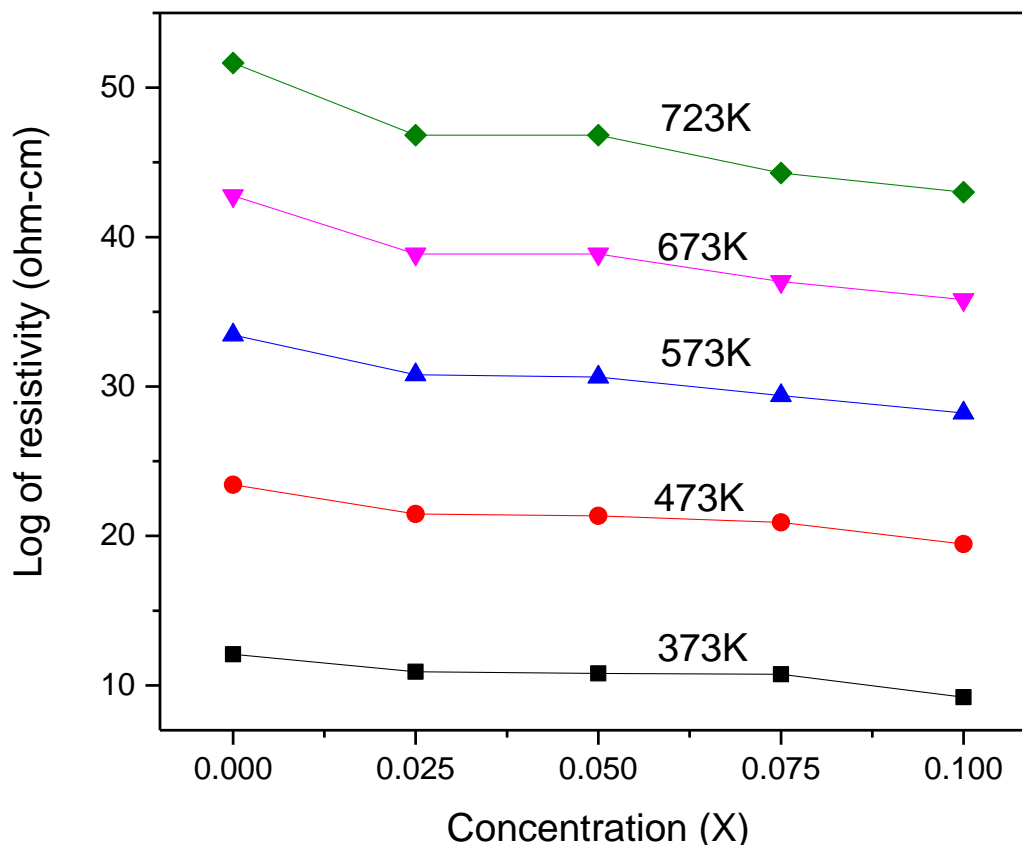


**Figure 8: Concentration vs log ( $\rho$ ) of Ni<sub>0.67</sub>Zn<sub>0.33</sub>Fe<sub>1.9</sub>Ho<sub>0.1-x</sub>Ce<sub>x</sub>O<sub>4</sub> (x = 0.00-0.1) ferrites**

#### 4. Conclusions

In summary, Ho and Ce doped Ni-Zn ferrite materials have been fabricated via self-ignited technique. XRD experiment confirmed the FCC spinel phase formation. A secondary phase observed from  $x = 0.025$  to  $x = 0.1$  due to the agglomeration of Ho and Ce ions at grain-boundaries. The lattice constant, X-ray, and bulk densities noticed to increase whereas porosity reduced with the increase in Ho<sup>3+</sup> and Ce<sup>3+</sup> contents in the spinel structure of Ni-Zn ferrites. FTIR spectroscopy revealed a clear change in vibrational bands with the substitution of Ho<sup>3+</sup> and Ce<sup>3+</sup> ions. The higher ionic radii of holmium and cerium deformed the centro-symmetric cubic structure which subsequently affect the entire polarization. Ac conductivity realized to increase up to  $x = 0.1$  while dissipation losses observed to decrease up to  $x = 0.1$  while The DC electrical resistivity is also increased by the addition of holmium and cerium ions.

#### References

- Abbas, S., Dixit, A., Chatterjee, R., & Goel, T. (2007). Complex permittivity, complex permeability and microwave absorption properties of ferrite-polymer composites. *Journal of Magnetism and Magnetic Materials*, 309(1), 20-24. doi:10.1016/j.jmmm.2006.06.006
- Akhter, S., & Hakim, M. (2010). Magnetic properties of cadmium substituted lithium ferrites. *Materials Chemistry and Physics*, 120(2-3), 399-403. doi:10.1016/j.matchemphys.2009.11.023
- Ali, I., Islam, M., Ishaque, M., Khan, H. M., Ashiq, M. N., & Rana, M. (2012). Structural and magnetic properties of holmium substituted cobalt ferrites synthesized by chemical co-precipitation method. *Journal of Magnetism and Magnetic Materials*, 324(22), 3773-3777. doi:10.1016/j.jmmm.2012.06.008

- Alone, S., Shirsath, S. E., Kadam, R., & Jadhav, K. (2011). Chemical synthesis, structural and magnetic properties of nano-structured Co–Zn–Fe–Cr ferrite. *Journal of Alloys and Compounds*, 509(16), 5055-5060. doi:10.1016/j.jallcom.2011.02.006
- Ashiq, M. N., Iqbal, M. J., & Gul, I. H. (2011). Effect of Al–Cr doping on the structural, magnetic and dielectric properties of strontium hexaferrite nanomaterials. *Journal of Magnetism and Magnetic Materials*, 323(3-4), 259-263. doi:10.1016/j.jmmm.2010.08.054
- AsifIqbal, M., Islam, M., Ali, I., Khan, M. A., Ramay, S. M., Khan, M. H., & Mehmood, M. K. (2017). Study of physical, magnetic and electrical properties of rare-earth substituted Li-Mg ferrites. *Journal of Alloys and Compounds*, 692, 322-331. doi:10.1016/j.jallcom.2016.09.049
- Cai, X., Wang, J., Li, B., Wu, A., Xu, B., Wang, B., . . . Li, Z. (2016). Microwave absorption properties of LiZn ferrites hollow microspheres doped with La and Mg by self-reactive quenching technology. *Journal of Alloys and Compounds*, 657, 608-615. doi:10.1016/j.jallcom.2015.10.153
- Cai, X., Xu, B., Wang, J., Li, B., Wu, A., Wang, B., . . . Li, Z. (2016). Effect of Ce and Mg doping on LiZn ferrites hollow microspheres prepared by self-reactive quenching technology. *Journal of Materials Science: Materials in Electronics*, 27(2), 1328-1336. doi:10.1007/s10854-015-3893-3
- Dar, M. A., Shah, J., Siddiqui, W., & Kotnala, R. (2012). Influence of synthesis approach on structural and magnetic properties of lithium ferrite nanoparticles. *Journal of Alloys and Compounds*, 523, 36-42. doi:10.1016/j.jallcom.2012.01.083
- Fang, X. S., Ye, C. H., Zhang, L. D., & Xie, T. (2005). Twinning-mediated growth of Al<sub>2</sub>O<sub>3</sub> nanobelts and their enhanced dielectric responses. *Advanced Materials*, 17(13), 1661-1665. doi:10.1002/adma.200401921
- Ferrites, M. M. (2012). Advances in magnetics. *IEEE Trans. Magn.*, 48, 1075.
- Haque, M. M., Huq, M., & Hakim, M. (2008). Densification, magnetic and dielectric behaviour of Cu-substituted Mg–Zn ferrites. *Materials Chemistry and Physics*, 112(2), 580-586. doi:j.matchemphys.2008.05.097
- Harrop, P., & Campbell, D. (1968). Selection of thin film capacitor dielectrics. *Thin Solid Films*, 2(4), 273-292. doi:10.1016/0040-6090(68)90034-5
- Hashim, M., Kumar, S., Koo, B., Shirsath, S. E., Mohammed, E., Shah, J., . . . Kumar, R. (2012). Structural, electrical and magnetic properties of Co–Cu ferrite nanoparticles. *Journal of Alloys and Compounds*, 518, 11-18. doi:10.1016/j.jallcom.2011.12.017
- Iqbal, M. A., Islam, M., Ali, I., Sadiq, I., & Ali, I. (2014). High frequency dielectric properties of Eu<sup>3+</sup>-substituted Li–Mg ferrites synthesized by sol–gel auto-combustion method. *Journal of Alloys and Compounds*, 586, 404-410. doi:10.1016/j.jallcom.2013.10.066
- Koops, C. (1951). On the dispersion of resistivity and dielectric constant of some semiconductors at audiofrequencies. *Physical review*, 83(1), 121. doi:10.1103/PhysRev.83.121
- Livingston, J. (1999). Electrical Insulation Conference/Electrical Manufacturing & Coil Winding'99 Expo October 28 through 28, 1999 Cincinnati Convention Center Cincinnati, Ohio USA.
- Manzoor, A., Khan, M. A., Shahid, M., & Warsi, M. F. (2017). Investigation of structural, dielectric and magnetic properties of Ho substituted nanostructured lithium ferrites synthesized via auto-citric combustion route. *Journal of Alloys and Compounds*, 710, 547-556. doi:10.1016/j.jallcom.2017.03.154
- Meena, R., Bhattacharya, S., & Chatterjee, R. (2010). Complex permittivity, permeability and microwave absorbing studies of (Co<sub>2</sub>– xMnx) U-type hexaferrite for X-band (8.2–12.4 GHz) frequencies. *Materials Science and Engineering: B*, 171(1-3), 133-138. doi:10.1016/j.mseb.2010.03.086
- Ramesh, M., Rao, G., Samatha, K., & Rao, B. P. (2015). Cation distribution of Ni–Cu substituted Li-ferrites. *Ceramics International*, 41(1), 1765-1770. doi:j.ceramint.2014.09.122
- Randhawa, B., & Singh, J. (2013). Physico-chemical studies on synthesis, characterization, and magnetic properties of Li–Ca–Zn nanoferrites. *Journal of nanoparticle research*, 15(1), 1-10. doi:10.1007/s11051-012-1351-1
- Rao, B. P., Kumar, A. M., Rao, K., Murthy, Y., Caltun, O., Dumitru, I., & Spinu, L. (2006). Synthesis and magnetic studies of Ni–Zn ferrite nanoparticles. *Journal of Optoelectronics and Advanced Materials*, 8(5), 1703-1705.

- Rezlescu, E., Rezlescu, N., Popa, P., Rezlescu, L., & Pasnicu, C. (1997). The influence of R<sub>2</sub>O<sub>3</sub> (R= Yb, Er, Dy, Tb, Gd, Sm and Ce) on the electric and mechanical properties of a nickel-zinc ferrite. *physica status solidi (a)*, 162(2), 673-678. doi:10.1002/1521-396X(199708)162:2<673::AID-PSSA673>3.0.CO;2-A
- Rezlescu, N., Rezlescu, E., Pasnicu, C., & Craus, M. (1994). Effects of the rare-earth ions on some properties of a nickel-zinc ferrite. *Journal of Physics: Condensed Matter*, 6(29), 5707.
- Sattar, A., El-Sayed, H., El-Shokrofy, K., & El-Tabey, M. (2005). Improvement of the magnetic properties of Mn-Ni-Zn Ferrite by the non magnetic Al-Ion substitution. *J. Appl. Sci*, 5(1), 162-168.
- Singh, N., Agarwal, A., & Sanghi, S. (2011). Dielectric relaxation, conductivity behavior and magnetic properties of Mg substituted Zn-Li ferrites. *Current applied physics*, 11(3), 783-789. doi:10.1016/j.cap.2010.11.073
- Srivastava, C., & Srinivasan, T. (1982). Effect of Jahn-Teller distortion on the lattice vibration frequencies of nickel ferrite. *Journal of Applied Physics*, 53(11), 8148-8150. doi:10.1063/1.330276
- Zhou, J.-P., Li, L., & Chen, X.-Z. (2010). Dielectric and magnetic properties of ZnO-doped cobalt ferrite. *Journal of Ceramic Processing Research*, 11(2), 263-272.